Waves and structural strain induced by a uniform current flow underneath a semi-infinite floating solar coverage

Yifeng Yang [1,2] and Luofeng Huang [2,*]

[1] *Department of Mechanical Engineering, University College London, London WC1E 7JE, United Kingdom*

[2] *Faculty of Engineering and Applied Sciences, Cranfield University, Cranfield MK43 0AL, United Kingdom*

(Received 4 December 2023; accepted 22 July 2024; published 20 September 2024)

Floating solar panels installed on water reservoirs will be an increasingly popular renewable energy scenario. However, a significant current flow will occur when the reservoir gate is open to release water. Such a current flow can cause complex fluid-structure interaction at the edge of the solar panels, reversely analogized to a ship advancing through calm water, signifying the generation of a stern wave. This wave can damage the solar panels, which needs to be investigated to ensure operational safety. In this context, the present paper analyzes a mixed boundary problem of a uniform flow passing through a two-dimensional semi-infinite elastic plate using an analytical approach—the Wiener-Hopf technique. The mathematical model is based on the linearized velocity potential for fluid flow and the Kirchhoff-Love plate theory for an elastic plate. Three different edge conditions are considered here, namely, clamped, simply supported, and free. Extensive results and discussions are provided for the amplitudes of the propagation wave, and principal strain in the elastic thin plate. In particular, significant "resonance" fluid-structure interactions are found when the current speed is at certain special magnitudes. To support straightforward industrial applications, these special flow rates are given as a water depth Froude number. Overall, this study can provide valuable insights for floating solar projects on water reservoirs to control the water-release rate, thus minimizing the potential structural problems.

DOI: 10.1103/PhysRevFluids.9.094804

I. INTRODUCTION

Solar photovoltaics is widely acknowledged as a pivotal technology for mitigating global carbon emissions. In contrast to other energy power plants, solar photovoltaic power generation is proportional to its surface coverage, necessitating a considerably large area to deploy an industrial-scale power plant [1]. One of the popular scenarios is to develop floating photovoltaics (FPV) on hydropower reservoirs, as shown in Fig. 1. On the one hand, such a configuration can utilize the water space [3], saving scarce land space for human activities, transportation, agriculture, natural reservation, etc. On the other hand, the proximity to the hydropower infrastructure allows solar farms to benefit from the existing power transmission and distribution networks, leading to cost savings. Almeida *et al.* [4] estimated that covering 10% of the world's hydropower reservoirs with FPV can bring about power generation equivalent to the sum of all current fossil fuel plants in the world, which attracts significant commercial and research interests.

Nevertheless, installing floating solar farms in hydropower reservoirs also entails a concern, which is related to a strong current flow underneath the solar panels when water is released from a reservoir. The flow can induce a wake at the solar farm edge, i.e., between covered and open water regions, which can cause a significant load and deformation on the solar panels [5], as shown in

*Contact author: luofeng.huang@cranfield.ac.uk

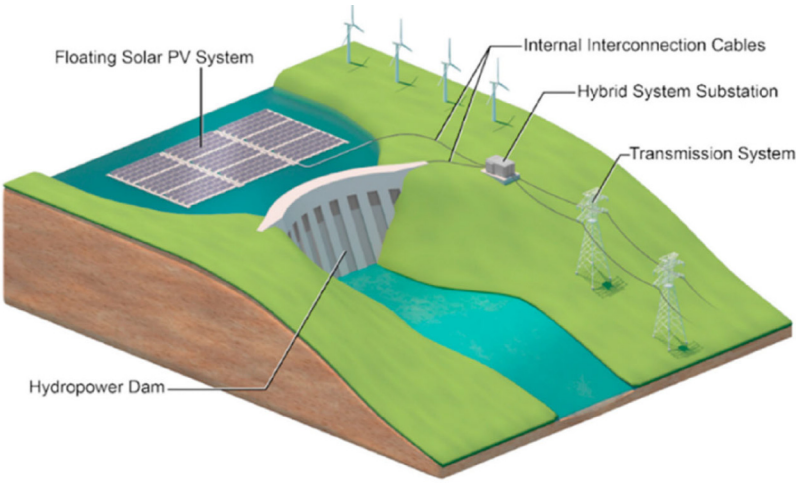

FIG. 1. Schematic of a hybrid FPV-hydropower system [2].

the sketch in Fig. 2. Hence, it is essential to investigate the interaction between such a flow and a floating solar farm.

In this context, the present work aims to establish an analytical model to explore the fluid-structure interaction of submerged water flow exiting from the edge of a floating solar power plant. Typically, a solar farm occupies a vast horizontal expanse, allowing the associated issues to be effectively addressed in a two-dimensional context [6]. The present article primarily focuses on the

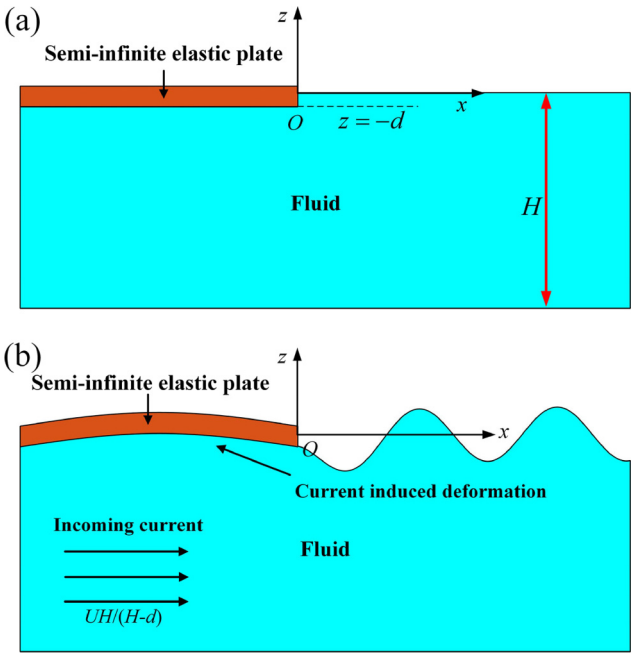

FIG. 2. Schematic of the case of the interaction between a semi-infinite elastic plate with an incoming current: (a) before the current coming into the system and (b) a steady state after the fluid and structural domains are coupled.

stern waves generated by the current at the floating platform's edge and the associated structural strain. In such a case, a semi-infinite elastic plate is employed as a viable model for simulating the solar farm. The potential flow theory is employed to predict the fluid field, and the structural deformation is modeled by the Kirchhoff-Love plate coupled with the fluid [7–9].

II. LITERATURE REVIEW

For solar photovoltaics covering a large horizontal area of the water surface, the motion and elasticity of the entire structure cannot be ignored when considering the influence of hydrodynamic loads [10–12]. In such a case, the thin elastic plate model for floating structures and linearized velocity potential theory for fluids are usually employed as one option to investigate such types of problems [13–16]. The present study modeled the solar farm as a semi-infinite elastic thin plate with an initial draft, and tried to understand its interaction with a uniform current, as a typical hydrodynamic problem for FPV on hydropower reservoirs. In the past decades, the theoretical model of a semi-infinite elastic plate was applied to the field of wave and sea ice interaction. For example, the problem of wave transmission and reflection by a semi-infinite ice sheet was solved by Fox and Squire [17] and Sahoo *et al.* [18] through the matched eigenfunction expansion (MEE), as well as by Balmforth and Craster [19] and Tkacheva [20] based on the Wiener-Hopf technique [21]. In their work [17–20], the plate was assumed to meet the water surface with zero draft, and edge conditions such as free were imposed on the edge of the plate. Later, Andrianov and Hermans [22] further considered a semi-infinite elastic plate with a finite draft, where the impermeable boundary condition was applied at the wetted surface of the plate edge. The nature of the works listed above is to understand how water waves propagate in elastic plates; because of the transition in the conditions at the plate edge, a key feature there is that the wave elevation and slope at this position may not be continuous. By contrast, the hydrodynamic load in the present study is a steady uniform current rather than an incident wave, which makes the problem steady instead of periodic and further leads to differences in the boundary conditions. In such a case, the former established methods in the literature may not be applied directly to the present problem. Besides, the steady wave profile here is generated by the incoming current being disturbed by the elastic plate. The flow separates from the side edge of the plate edge [23,24], and additional conditions may need to be applied to ensure the flow separation effects, which is quite different from the treatment in the previous periodic problems.

Apart from the works with a semi-infinite elastic plate, this study is also related to hydroelastic waves generated by a moving load or an incoming current. For example, Davys *et al.* [25] and Milinazzo *et al.* [26] investigated the linearized problem of waves generated by a steadily moving object on a floating elastic plate by using the Fourier transform method. Guyenne and Parau [27] further considered the nonlinear elastic plate condition and solved it via a boundary integral equation based on Cauchy's integral formula. Besides, Li *et al.* [28] considered steady waves due to a uniform current disturbed by a circular cylinder submerged below an elastic plate, based on the Green's function approach. Lustri [29] studied the nonlinear hydroelastic waves generated by flow over submerged obstacles, where an exponential asymptotic analysis was employed to derive the solution. In these works, the elastic plate is perfect and assumed to be infinitely extended; the present work aims to understand how steady waves present in a semi-infinite elastic plate, and to illustrate the influence of the plate edge.

The study in this paper is also related to stern waves due to a current passing underneath a rigid floating structure. Over the past few decades, numerous studies have been conducted to understand the characteristics of stern waves of floating rigid bodies. Haussling [23] and Schmidt [24] investigated the stern waves of a two-dimensional semi-infinite extended rigid plate of infinite water depth, where Haussling [23] studied the cases both with linear and nonlinear free surface boundary conditions numerically, and Schmidt [24] addressed the linearized problem for a series of distinctive shapes of the rigid plate. Later, McCue and Stump [30] solved the problem of linear stern waves of finite water depth analytically based on the Wiener-Hopf technique, and pointed

out that a nonsingular solution only exists when the water-depth-based Froude number is less than 1. Subsequently, Maleewong and Grimshaw [31] extended the problem to nonlinear free surface boundary conditions and considered a wide range of drafts by using a boundary integral method; they indicated that the results of the linear and nonlinear approaches were in good agreement when the draft of the rigid plate was much less than the mean water depth. Binder [32] considered stern waves of a curved rigid plate with a specific shape, and a weakly nonlinear solution based on a Korteweg–De Vries (KdV) equation was derived analytically. Later, Ogilat *et al.* [33] further extended it to more general shapes of curved rigid plates. In their work, an approach that combined the Wiener-Hopf technique and conformal mapping was proposed to solve the linear problem, and a nonlinear analysis based on the KdV equation [32] was provided. The works discussed here are all for stern waves behind a semi-infinite rigid plate. However, on occasions when the horizontal dimension of the floating structure is significant, like the present floating solar farm, the model of a rigid plate may not be reasonable, because considerable deformations and strain of the structure induced by hydrodynamic loads should be considered. Hence, the model of a semi-infinite elastic plate will be employed in this article to extend the previous research about a rigid plate. Since the elasticity of the plate is considered as an additional factor, the induced structural deformation may make the characteristic of stern waves quite different from that of a rigid plate. Through the enhanced solution, the present work aims to shed some light on this fluid-structural physics problem as well as the industrial application of floating solar farms on water reservoirs.

The rest of the paper is organized as follows. In Sec. III, the mathematical model of the problem is established based on the linearized velocity potential theory and Kirchhoff-Love plate theory. The solution procedure of the Wiener-Hopf technique is given in Sec. IV. Systematic result analyses in different boundary and flow conditions are presented in Sec. V, followed by the conclusions in Sec. VI.

III. PROBLEM DESCRIPTION

We may consider the interaction between a uniform current and a two-dimensional semi-infinite elastic plate with an initial draft, as sketched in Fig. 2. In Fig. 2(a), a Cartesian coordinate system O-xz is defined with the x axis along the undisturbed surface, and the z axis pointing upwards. The elastic plate covers the region at $x < 0$ and its lower surface is along $z = -d$, while the region at $x > 0$ is with the free surface boundary condition. The bottom of the fluid is along $z = -H$. At one time point, there is a uniform current coming from $x = -\infty$ to $x = +\infty$; we may assume that the current speed far downstream is denoted by U. Since the mean water depth at $x < 0$ has been narrowed as $H-d$ because of the existence of the plate, based on the conservation of mass, the speed of the current far upstream should be $UH/(H-d)$. The semi-infinite elastic plate will be disturbed by the current and experience an oscillation. After a sufficiently long time, a steady state of the flow field will be reestablished, where a steady wave profile may be generated along the water surface, as shown in Fig. 2(b).

In the present problem, the fluid is assumed to be inviscid and incompressible and its motion is irrotational. Since the problem is steady and independent of time, a velocity potential $\Phi(x, z)$ will be introduced to describe the motion of the fluid. We may split Φ into a summation of the steady current component and the disturbed component, which provides

$$\Phi(x, z) = \frac{UH}{H - d}x + \phi(x, z), \tag{1}$$

where $\phi(x, z)$ is governed by the Laplace equation in the entire fluid domain as

$$\frac{\partial^2 \phi}{\partial x^2} + \frac{\partial^2 \phi}{\partial z^2} = 0. \tag{2}$$

The dynamic and kinematic boundary conditions on the elastic plate can be written as [28,34]

$$L\frac{d^4W}{dx^4} = p, \quad \text{at} \quad x < 0, \quad z = -d + W(x), \tag{3a}$$

$$\frac{\partial \Phi}{\partial z} = \frac{\partial \Phi}{\partial x}\frac{dW}{dx}, \quad \text{at} \quad x < 0, \quad z = -d + W(x), \tag{3b}$$

where the terms of temporal derivatives in Eqs. (3) are omitted because the problem is steady, L denotes the flexural rigidity of the elastic plate, $W(x)$ represents the wave elevation measured from the initial undisturbed lower surface of the plate, or $z = -d$ at $x < 0$, and it is measured from the undisturbed water surface, or $z = 0$ at $x > 0$. $p(x)$ denotes the hydrodynamic pressure, which can be calculated from the Bernoulli equation as

$$p(x) = -\rho\left[\frac{1}{2}\left(\nabla\Phi\cdot\nabla\Phi - \frac{U^2H^2}{(H-d)^2}\right) + gW\right], \quad x < 0, \tag{4}$$

where ρ is the density of the fluid and g denotes the acceleration due to gravity. The dynamic free surface boundary condition at $x > 0$ can be expressed as [30]

$$\tfrac{1}{2}(\nabla\Phi\cdot\nabla\Phi - U^2) + gW = 0 \quad \text{at } x > 0,\ z = W(x). \tag{5}$$

Besides, the kinematic boundary condition in Eq. (3b) should also be satisfied at $x > 0$ and $z = W(x)$. The impermeable condition at the bottom of the fluid gives

$$\frac{\partial \phi}{\partial z} = 0, \quad z = -H. \tag{6}$$

At the edge of the elastic plate, suitable edge conditions should be imposed, with the aim to simulate the physical constraints at the edge of the floating solar farm [35]. Here, three commonly used theoretical types are considered. In particular, the clamped edge is to let the deflection and slope of the plate be zero, which can be used to model the edge of the floating solar farm that is fully fixed. The simply supported edge is to let the deflection and bending moment be zero. The free edge is to let the shear force and bending moment be zero, or no external constraint is applied to the edge of the solar panel. From Timoshenko and Woinowsky-Krieger [36], we obtain

$$W(0^-) = 0 \quad \text{and} \quad \frac{dW}{dx}(0^-) = 0, \quad \text{clamped}, \tag{7a}$$

$$W(0^-) = 0 \quad \text{and} \quad \frac{d^2W}{dx^2}(0^-) = 0, \quad \text{simply supported}, \tag{7b}$$

$$\frac{d^2W}{dx^2}(0^-) = 0 \quad \text{and} \quad \frac{d^3W}{dx^3}(0^-) = 0, \quad \text{free}. \tag{7c}$$

Based on the discussion in Refs. [37,38], we may further assume that the flow at the sharp edge of the plate separates smoothly and tangentially, which is used to require the velocity at the edge to be finite. In such a case, apart from the structural edge conditions in Eqs. (7), the Kutta condition should also be imposed to ensure the continuity of the wave elevation and slope. Hence, we have

$$-d + W(0^-) = W(0^+), \tag{8a}$$

$$\frac{dW(0^-)}{dx} = \frac{dW(0^+)}{dx}. \tag{8b}$$

It should be noted again that the use of the Kutta condition is valid when the current speed is not very low. As discussed in Ref. [39], the flow will separate from the lower edge point of the plate when the draft-based Froude number $F_T = U/\sqrt{gd}$ is greater than a critical value, which is around 2. When $U \to 0$ or is very small, the separation point is located at the side edge, and the flow may be unstable. In such a case, Eqs. (8) may be invalid. Normally, when a dam releases water, the speed of the flow, U, can be more than 10 m/s [40], for a typical solar panel with a draft d of 0.1 m [3],

which gives a transom-draft Froude number F_T of more than 10, and the Kutta condition can be applied to the present problem.

The far-field condition should also be applied at $x \to \pm\infty$, which gives

$$\frac{\partial \phi}{\partial x} \to w_{\pm}(x, z) \quad \text{as} \quad x \to \pm\infty, \tag{9}$$

where $w_{\pm}(x, z)$ denote wavy functions oscillatory with x at $x \to \pm\infty$, and its expression depends on the group velocity of the propagating waves at infinity. If the group velocity of the wave component is larger or smaller than the current speed U, the waves will show in the downstream ($x = -\infty$) or upstream ($x = +\infty$) region correspondingly.

Before analyzing this boundary value problem, a series of nondimensional variables is defined based on the density of the fluid, ρ, the acceleration due to gravity, g, as well as the mean water depth H. In particular, $x' = x/H$, $z' = z/H$, $\Phi' = \Phi/H\sqrt{gH}$, $W' = W/H$, and $\epsilon = d/H$ and the water-depth-based Froude number is $F = U/\sqrt{gH}$. In the following text, the prime in these variables will be omitted and all the parameters are presented in a nondimensional form. In such a case, Eqs. (1), (3a), (4), (5), and (8) can be reexpressed as

$$\Phi(x, z) = \frac{F}{1-\epsilon}x + \phi(x, z), \tag{10}$$

$$D\frac{d^4 W}{dx^4} = p \quad \text{at} \quad x < 0, \quad z = -\epsilon + W(x), \tag{11}$$

where $D = L/\rho g H^4$, and

$$p(x) = -\left[\frac{1}{2}\left(\nabla\Phi \cdot \nabla\Phi - \frac{F^2}{(1-\epsilon)^2}\right) + W\right], \quad x < 0. \tag{12}$$

$$\frac{1}{2}(\nabla\Phi \cdot \nabla\Phi - F^2) + W = 0 \quad \text{at } x > 0, \quad z = W(x). \tag{13}$$

$$-\epsilon + W(0^-) = W(0^+) \tag{14a}$$

$$\frac{dW(0^-)}{dx} = \frac{dW(0^+)}{dx}. \tag{14b}$$

Additionally, Eqs. (2), (7), and (9) remain in the same formats; Eq. (3b) should be revised to be satisfied at $x < 0$ and $z = -\epsilon + W(x)$ and at $x > 0$ and $z = W(x)$; and Eq. (6) should be satisfied along $z = -1$.

Here, we consider the case of the draft much less than the mean water depth, or $\epsilon \ll 1$. In such a case, the velocity potential $\phi(x, z)$ and wave elevation $W(x)$ may be written in the following perturbation form of ϵ:

$$\phi(x, z) = \epsilon\phi_1(x, z) + O(\epsilon^2) \tag{15a}$$

$$W(x) = \epsilon\eta_1(x) + O(\epsilon^2), \tag{15b}$$

where $\phi_1(x, z)$ and $\eta_1(x)$ represent the first-order component of velocity potential and wave elevation, respectively. We substitute Eqs. (15) into Eqs. (3b), (11), and (12), and then apply the Taylor series at $z = 0$, eliminating η_1 from the obtained equations. The boundary condition for ϕ_1 at $x < 0$ and $z = 0$ is obtained as

$$\left(D\frac{\partial^4}{\partial x^4} + 1\right)\frac{\partial \phi_1}{\partial z} + F^2\frac{\partial^2 \phi_1}{\partial x^2} = 0, \quad x < 0, \quad z = 0. \tag{16}$$

Similarly, the boundary conditions for ϕ_1 at $x > 0$ and $z = 0$ provide

$$\frac{\partial \phi_1}{\partial z} + F^2\frac{\partial^2 \phi_1}{\partial x^2} = 0, \quad x > 0, \quad z = 0. \tag{17}$$

Following the procedure above, $\eta_1(x)$ can be expressed as

$$\eta_1(x) = \begin{cases} -\frac{D}{F}\frac{\partial^4\phi_1(x,0)}{\partial x^3\partial z} - F\frac{\partial\phi_1(x,0)}{\partial x}, & x < 0 \\ -F\left[F + \frac{\partial\phi_1(x,0)}{\partial x}\right], & x > 0. \end{cases} \tag{18}$$

In such a case, the edge conditions in Eqs. (7) should be satisfied by $\eta_1(x)$. Besides, substituting Eq. (15b) into Eq. (14), the Kutta condition provides

$$-1 + \eta_1(0^-) = \eta_1(0^+), \tag{19a}$$

$$\frac{d\eta_1(0^-)}{dx} = \frac{d\eta_1(0^+)}{dx}. \tag{19b}$$

The governing equation in Eq. (2), as well as the boundary conditions in Eqs. (16)–(19) and (7) construct the boundary value problem for ϕ_1. The Kutta condition in Eqs. (19) shows a key difference with the problem of wave diffraction by a semi-infinite elastic plate [19,20], where only two conditions at the plate edge can lead to a unique solution, and discontinuity on the wave elevation and slope are allowed at the edge. By contrast, two additional conditions are needed here to ensure the continuity of the flow due to flow separation.

IV. SOLUTION PROCEDURE

A. Derivation of the solution through the Wiener-Hopf technique

The boundary value problem for ϕ_1 established in Sec. III can be solved by the Jones' version of the Wiener-Hopf technique [21]. The following Fourier transforms are defined with the complex-valued variable α,

$$\hat{\phi}_+(\alpha, z) = \int_0^{+\infty} \phi_1(x, z)e^{i\alpha x}dx, \tag{20a}$$

$$\hat{\phi}_-(\alpha, z) = \int_{-\infty}^{0} \phi_1(x, z)e^{i\alpha x}dx, \tag{20b}$$

$$\hat{\phi}(\alpha, z) = \hat{\phi}_+(\alpha, z) + \hat{\phi}_-(\alpha, z). \tag{21}$$

The functions $\hat{\phi}_+(\alpha, z)$ and $\hat{\phi}_-(\alpha, z)$ are defined in the upper ($\mathrm{Im}\{\alpha\} > 0$) and lower ($\mathrm{Im}\{\alpha\} < 0$) complex planes of α, respectively, and they can be defined over the entire complex plane through analytical continuation. In addition to a couple of singularities at the real axis of α, $\hat{\phi}_+(\alpha, z)$ and $\hat{\phi}_-(\alpha, z)$ are analytical in the half-planes $\mathrm{Im}\{\alpha\} > 0$ and $\mathrm{Im}\{\alpha\} < 0$, respectively. It should be noted that these poles at the real axis of α correspond to propagation waves at $x = \pm\infty$; the distributions of these poles are related to the Froude number F, which will be given in detail later.

Applying Eqs. (20) and (21) to Eq. (2), together with the boundary condition in Eqs. (6), $\hat{\phi}(\alpha, z)$ can be solved as

$$\hat{\phi}(\alpha, z) = A(\alpha)Z(z, \alpha), \tag{22}$$

where $A(\alpha)$ is an unknown function of α and

$$Z(z, \alpha) = \cosh\alpha(z + 1). \tag{23}$$

Substituting Eqs. (20) and (21) into Eqs. (16) and (17), we obtain

$$C_+(\alpha) + C_-(\alpha) = A(\alpha)\alpha^2 K_1(\alpha, F), \tag{24}$$

$$D_+(\alpha) + D_-(\alpha) = A(\alpha)\alpha^2 K_2(\alpha, F), \tag{25}$$

where $C_\pm(\alpha)$ and $D_\pm(\alpha)$ are obtained by applying a half-range Fourier transform in Eqs. (20a) and (20b) to Eqs. (16) and (17), respectively. $K_1(\alpha, F)$ and $K_2(\alpha, F)$ denote the dispersion equations

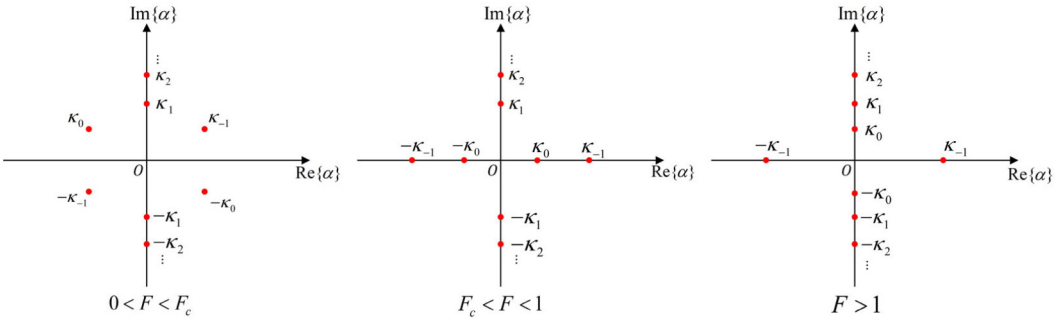

FIG. 3. Distribution of the roots of $K_1(\alpha, F) = 0$ in the entire complex plane of α.

corresponding to cases fully covered by an elastic plate and without the elastic plate (free surface case), respectively, where

$$K_1(\alpha, F) = (D\alpha^4 + 1)\frac{\sinh\alpha}{\alpha} - F^2\cosh\alpha, \tag{26a}$$

$$K_2(\alpha, F) = \frac{\sinh\alpha}{\alpha} - F^2\cosh\alpha. \tag{26b}$$

Notice that $\phi_1(x, z)$ satisfies Eq. (16) at $x < 0$ and Eq. (17) at $x > 0$. In such a case, we have $C_-(\alpha) = D_+(\alpha) = 0$. We may eliminate $A(\alpha)$ from Eqs. (24) and (25), which provides

$$\frac{C_+(\alpha)}{D_-(\alpha)} = \frac{K_1(\alpha, F)}{K_2(\alpha, F)} = K(\alpha, F). \tag{27}$$

Following the general steps of the Wiener-Hopf technique, $K(\alpha, F)$ needs to be factorized as

$$K(\alpha, F) = K_+(\alpha, F)K_-(\alpha, F), \tag{28}$$

where $K_\pm(\alpha, F)$ is analytical in the same domains as $\hat{\phi}_\pm(\alpha, F)$, respectively. To do that, the distribution of the roots of $K_1(\alpha, F) = 0$ and $K_2(\alpha, F) = 0$ should be introduced first. Based on the discussion in Ref. [41], $K_1(\alpha, F) = 0$ has an infinite number of roots at $\alpha = \pm\kappa_m$ ($m = -1, 0, 1, \ldots$), and the distribution of these roots is related to the Froude number F. As shown in Fig. 3, there is a critical Froude number F_c, at which $K_2(\alpha, F_c) = 0$ will have a double real root $\alpha = \kappa_c$ and satisfy $\frac{\partial K_2(\kappa_c, F_2)}{\partial\alpha} = 0$ [28]. When $0 < F < F_c$, κ_{-1} and κ_0 are two fully complex roots satisfying $\kappa_0 = -\bar{\kappa}_{-1}$ where $\mathrm{Re}\{\kappa_{-1}\} > 0$, $\mathrm{Im}\{\kappa_{-1}\} > 0$, κ_m ($m = 1, 2, 3, \ldots$) are purely positive imaginary roots, and $\kappa_m \in (m\pi\mathrm{i}, m\pi\mathrm{i} + \frac{\pi}{2}\mathrm{i})$. When $F_c < F < 1$, κ_{-1} and κ_0 become two purely positive real roots with $\kappa_{-1} > \kappa_0$, while κ_m ($m = 1, 2, 3, \ldots$) remains to be an imaginary root. When $F > 1$, κ_0 further becomes a purely imaginary root and $\kappa_0 \in (0, \frac{\pi}{2}\mathrm{i})$. By contrast, $K_2(\alpha, F) = 0$ also has an infinite number of roots at $\alpha = \pm\hbar_m$ ($m = 0, 1, 2, \ldots$). As presented in Fig. 4, $\hbar_0$ denotes a purely positive real root when $0 < F < 1$. When $F > 1$, $\hbar_0$ becomes a purely imaginary root and $\hbar_0 \in (0, \frac{\pi}{2}\mathrm{i})$. $\hbar_m$ ($m = 1, 2, 3, \ldots$) are always purely positive imaginary roots with $\hbar_m \in (m\pi\mathrm{i}, m\pi\mathrm{i} + \frac{\pi}{2}\mathrm{i})$.

Thus, based on the Weierstrass factorization, $K(\alpha, F)$ can be written as

$$K(\alpha, F) = \frac{\kappa_{-1}^2\kappa_0^2(\hbar_0^2 - \alpha^2)}{\hbar_0^2(\kappa_{-1}^2 - \alpha^2)(\kappa_0^2 - \alpha^2)}\prod_{m=1}^{+\infty}\frac{\hbar_m^2(\kappa_m^2 - \alpha^2)}{\kappa_m^2(\hbar_m^2 - \alpha^2)}. \tag{29}$$

To factorize $K(\alpha, F)$, it can be known that terms $(\alpha \pm \kappa_m)$ and $(\alpha \pm \hbar_m)$ ($m = 1, 2, 3, \ldots$) must be in $K_\pm(\alpha, F)$, respectively, because $K_+(\alpha, F)$ and $K_-(\alpha, F)$ should be analytical in the upper ($\mathrm{Im}\{\alpha\} > 0$) and lower ($\mathrm{Im}\{\alpha\} < 0$) complex planes of α and do not have zeros, respectively. Thus,

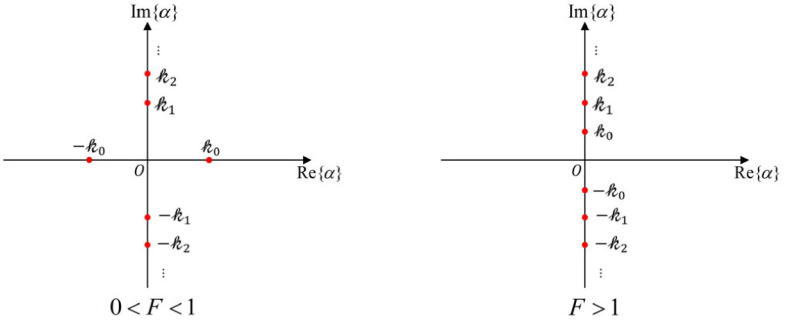

FIG. 4. Distribution of the roots of $K_2(\alpha, F) = 0$ in the entire complex plane of α.

we may write

$$K_{\pm}(\alpha, F) = g_{\pm}(\alpha, F) \prod_{m=1}^{+\infty} \left[\frac{\hbar_m(\kappa_m \pm \alpha)}{\kappa_m(\hbar_m \pm \alpha)} \right], \tag{30}$$

where $g_+(\alpha, F)g_-(\alpha, F) = \frac{\kappa_{-1}^2\kappa_0^2(\hbar_0^2-\alpha^2)}{\hbar_0^2(\kappa_{-1}^2-\alpha^2)(\kappa_0^2-\alpha^2)}$ corresponds to terms of propagating waves. Physically, the distribution of propagating waves should be based on their group velocities. As discussed in Ref. [42] for the free surface case, when $\hbar_0$ is real, it corresponds to a propagation wave in the downstream region ($x = +\infty$) since its group velocity is less than the speed of the incoming flow. By contrast, as demonstrated by Li *et al.* [28] for the case fully covered by an ice sheet, when κ_{-1} and κ_0 are real, κ_{-1} corresponds to a propagation wave in the upstream region ($x = -\infty$) since its group velocity is larger than the speed of the incoming flow, whereas κ_0 pertains to a propagation wave in the downstream region ($x = +\infty$). Mathematically, when performing the inverse Fourier transform on $\hat{\phi}$, the integral path from $\alpha = -\infty$ to $\alpha = +\infty$ should pass over the poles at $\alpha = \pm\hbar_0$, $\alpha = \pm\kappa_0$ and pass under the poles at $\alpha = \pm\kappa_{-1}$. Based on the above discussion, $g_{\pm}(\alpha, F)$ should be factorized as

$$g_+(\alpha, F) = \begin{cases} \frac{\hbar_0^2(\kappa_{-1}+\alpha)(\kappa_0+\alpha)}{\kappa_{-1}\kappa_0(\hbar_0^2-\alpha^2)}, & 0 < F < F_c \\ \frac{\hbar_0^2(\kappa_0^2-\alpha^2)}{\kappa_0^2(\hbar_0^2-\alpha^2)}, & F_c < F < 1 \\ \frac{\hbar_0(\kappa_0+\alpha)}{\kappa_0(\hbar_0+\alpha)}, & F > 1, \end{cases} \tag{31}$$

$$g_-(\alpha, F) = \begin{cases} \frac{(\kappa_{-1}-\alpha)(\kappa_0-\alpha)}{\kappa_{-1}\kappa_0}, & 0 < F < F_c \\ \frac{(\kappa_{-1}^2-\alpha^2)}{\kappa_{-1}^2}, & F_c < F < 1 \\ \frac{\hbar_0(\kappa_{-1}^2-\alpha^2)(\kappa_0-\alpha)}{\kappa_{-1}^2\kappa_0(\hbar_0-\alpha)}, & F > 1. \end{cases} \tag{32}$$

From the analysis above, we may define

$$\gamma = \begin{cases} \min\{\mathrm{Im}\{\kappa_{-1}\}, |\kappa_1|, |\hbar_1|\}, & 0 < F < F_c \\ \min\{|\kappa_1|, |\hbar_1|\}, & F_c < F < 1 \\ \min\{|\kappa_0|, |\hbar_0|\}, & F > 1 \end{cases} \tag{33}$$

and further introduce $S_{\pm}$ in the complex plane of α, where S_+ denotes the plane with $\mathrm{Im}\{\alpha\} > -\gamma$ except for the points at $\alpha = \pm\kappa_0$ and $\alpha = \pm\hbar_0$ when κ_0 and $\hbar_0$ are real. S_- represents the region with $\mathrm{Im}\{\alpha\} < \gamma$ except for the points at $\alpha = \pm\kappa_{-1}$ when κ_{-1} is real. A sketch of regions $S_{\pm}$ at different F is given in Fig. 5. From Eqs. (30)–(33), it can be known that $\hat{\phi}_{\pm}(\alpha, z)$ and $K_{\pm}(\alpha, F)$ are analytical in the regions $S_{\pm}$, respectively. Once $K_{\pm}(\alpha, F)$ are obtained, substituting Eq. (28) into

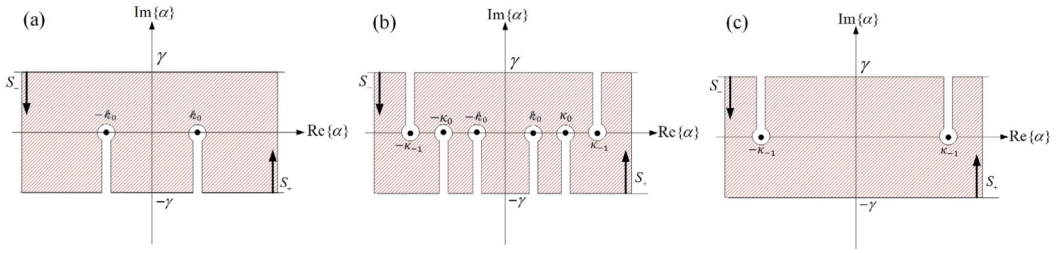

FIG. 5. A sketch of the domains of S_+ and S_-: (a) $0 < F < F_c$, (b) $F_c < F < 1$, and (c) $F > 1$.

Eq. (27), we have

$$\frac{C_+(\alpha)}{K_+(\alpha, F)} = D_-(\alpha)K_-(\alpha, F). \tag{34}$$

It can be found that the functions on the left- and right-hand sides of Eq. (34) are analytical in the complex domains S_+ and S_-, respectively. Notice from Fig. 5 that S_+ and S_- have an overlapping area in the complex plane of α. Based on the theorem of analytical continuation, the functions on the left- and right-hand sides must be identical and analytical in the entire complex plane. Furthermore, using the Liouville theorem, such a function can only be polynomial as $2\pi Q(\alpha)$, which gives

$$\frac{C_+(\alpha)}{K_+(\alpha, F)} = 2\pi Q(\alpha), \tag{35a}$$

$$D_-(\alpha)K_-(\alpha, F) = 2\pi Q(\alpha). \tag{35b}$$

Substituting Eq. (34) into Eqs. (24) and (25), $A(\alpha)$ can be written as

$$A(\alpha) = \frac{2\pi Q(\alpha)K_+(\alpha, F)}{\alpha^2 K_1(\alpha, F)} = \frac{2\pi Q(\alpha)}{\alpha^2 K_2(\alpha, F)K_-(\alpha, F)}. \tag{36}$$

Applying Eq. (36) to Eq. (22) provides

$$\hat{\phi}(\alpha, z) = \frac{2\pi Q(\alpha)K_+(\alpha, F)Z(z, \alpha)}{\alpha^2 K_1(\alpha, F)}. \tag{37}$$

$\phi_1(x, z)$ can be derived by performing the inverse Fourier transform to Eq. (37), which gives

$$\phi_1(x, z) = \frac{1}{2\pi}\int_{-\infty}^{+\infty} \hat{\phi}(\alpha, z)e^{-i\alpha x}d\alpha = \int_{-\infty}^{+\infty} \frac{Q(\alpha)K_+(\alpha, F)Z(z, \alpha)}{\alpha^2 K_1(\alpha, F)}e^{-i\alpha x}d\alpha. \tag{38}$$

It can be found from Eq. (37) that there will be a pole at $\alpha = 0$ in $\hat{\phi}(\alpha, z)$ if $Q(0)$ or $Q'(0)$ is nonzero. Based on the analysis in Ref. [30], there should be no mean wave elevation at the region $x < 0$, which means the residue at $\alpha = 0$ in Eq. (38) should be included in $\phi(x, z)$ only when $x > 0$. Hence, the integral path from $\alpha = -\infty$ to $\alpha = +\infty$ in Eq. (38) should pass over the singularity at $\alpha = 0$. Besides, as mentioned above, the integral path should also pass over the poles at $\alpha = \pm k_0$ when $0 < F < 1$, and pass under the poles at $\alpha = \pm\kappa_{-1}$ when $F > F_c$. Applying Eq. (38) to Eqs. (18), $\eta_1(x)$ can be expressed as

$$\eta_1(x) = \begin{cases} -\frac{i}{F}\int_{-\infty}^{+\infty} \frac{Q(\alpha)K_+(\alpha,F)[D\alpha^3 \sinh\alpha(z+1) - F^2\cosh\alpha(z+1)]}{\alpha K_1(\alpha,F)}e^{-i\alpha x}d\alpha, & x < 0 \\ iF\int_{-\infty}^{+\infty} \frac{Q(\alpha)\cosh\alpha(z+1)}{\alpha K_-(\alpha,F)K_2(\alpha,F)}e^{-i\alpha x}d\alpha - F^2, & x > 0, \end{cases} \quad z \to 0^-. \tag{39a,b}$$

We may further apply the theorem of residue to Eqs. (39) and, using the zeros of Eqs. (26), notice $K_1(\alpha,F)/K_2(\alpha,F)=K_+(\alpha,F)K_-(\alpha,F)$, which provides

$$\eta_1(x)=-\frac{2\pi}{F}\sum_{\zeta\in R_+}\frac{Q(\zeta)K_+(\zeta,F)\sinh\zeta}{\zeta^2K_1^{'}(\zeta,F)}e^{-\mathrm{i}\zeta x}\quad x<0 \tag{40a}$$

$$\eta_1(x)=\frac{2\pi}{F}\sum_{\zeta\in Q_-}\frac{Q(\zeta)\sinh\zeta}{\zeta^2K_2^{'}(\zeta,F)K_-(\zeta,F)}e^{-\mathrm{i}\zeta x}+\frac{2\pi F}{1-F^2}Q(0)-F^2\quad x>0, \tag{40b}$$

where $K_i^{'}(\alpha,F)$ $(i=1,2)$ represents the derivative of $K_i(\alpha,F)$ with respect to α. R_+ and Q_- are the sets defined as

$$R_+=\begin{cases}\{\kappa_m|m=-1,0,1\ldots\} & 0<F<F_c\\ \{\kappa_m|m=1,2,3\ldots\}\cup\{\pm\kappa_{-1}\} & F_c<F<1\\ \{\kappa_m|m=0,1,2\ldots\}\cup\{\pm\kappa_{-1}\} & F>1\end{cases}, \tag{41}$$

$$Q_-=\begin{cases}\{-\mathscr{k}_m|m=1,2,3\ldots\}\cup\{\pm\mathscr{k}_0\} & 0<F<1\\ \{-\mathscr{k}_m|m=0,1,2\ldots\} & F>1\end{cases}. \tag{42}$$

It should be noted that $\frac{2\pi F}{1-F^2}Q(0)$ in Eq. (40b) is the term induced by the residue at $\alpha=0$. From Eqs. (40), $\eta_1(x)$ can be further simplified as

$$\eta_1(x)=\begin{cases}\frac{\mathrm{i}}{F}\int_{-\infty}^{+\infty}\frac{Q(\alpha)K_+(\alpha,F)\sinh\alpha}{\alpha^2K_1(\alpha,F)}e^{-\mathrm{i}\alpha x}d\alpha, & x<0\\ \frac{\mathrm{i}}{F}\int_{-\infty}^{+\infty}\frac{Q(\alpha)\sinh\alpha}{\alpha^2K_2(\alpha,F)K_-(\alpha,F)}e^{-\mathrm{i}\alpha x}d\alpha-\frac{2\pi}{F}Q(0)-F^2, & x>0.\end{cases} \tag{43a,b}$$

It should be noted that the integral path in Eq. (43) is the same as that in Eq. (38). Based on a similar analysis in Ref. [41], it can be shown that $|K_+(\alpha,F)|\sim O(|\alpha|^{0.5})$ and $|K_-(\alpha,F)|\sim O(|\alpha|^{2.5})$ as $\alpha\to\pm\infty$. To ensure the convergence of the integral in Eqs. (43), $Q(\alpha)$ should be at most a cubic function as

$$Q(\alpha)=c_0+c_1\alpha+c_2\alpha^2+c_3\alpha^3. \tag{44}$$

Substituting Eq. (44) into Eqs. (43), and noticing $K_1(\alpha,F)/K_2(\alpha,F)=K_+(\alpha,F)K_-(\alpha,F)$ again, we have

$$\eta_1(x)=c_0I(x)+\mathrm{i}c_1I^{(1)}(x)-c_2I^{(2)}(x)-\mathrm{i}c_3I^{(3)}(x)-H(x)\left(\frac{2\pi}{F}c_0+F^2\right), \tag{45}$$

where

$$I(x)=\frac{\mathrm{i}}{F}\int_{-\infty}^{+\infty}\frac{K_+(\alpha,F)\sinh\alpha}{\alpha^2K_1(\alpha,F)}e^{-\mathrm{i}\alpha x}d\alpha, \tag{46}$$

$I^{(n)}(x)$ denotes the nth derivatives of $I(x)$ with respect to x, and $H(x)$ denotes the Heaviside step function. The computations of $I^{(n)}(0^+)$ and $I^{(n)}(0^-)$ are given in Appendix A. Applying the Kutta conditions in Eqs. (19a) and (19b) to Eq. (45), as well as using $I^{(n)}(0^-)=I^{(n)}(0^+)$ for $n\leqslant 3$ and $I^{(4)}(0^+)\to\infty$ obtained in Appendix A, provides

$$c_0=\frac{F(1-F^2)}{2\pi}, \tag{47a}$$

$$c_3=0. \tag{47b}$$

Applying the edge conditions in Eqs. (7) to Eq. (45) and using Eqs. (47), the following results can be obtained. For the clamped edge:

$$c_1=-\frac{F(1-F^2)}{2\pi\mathrm{i}}\frac{I^{(1)}(0^-)I^{(2)}(0^-)-I(0^-)I^{(3)}(0^-)}{[I^{(2)}(0^-)]^2-I^{(1)}(0^-)I^{(3)}(0^-)}, \tag{48a}$$

$$c_2 = -\frac{F(1-F^2)}{2\pi}\frac{[I^{(1)}(0^-)]^2 - I(0^-)I^{(2)}(0^-)}{[I^{(2)}(0^-)]^2 - I^{(1)}(0^-)I^{(3)}(0^-)}. \tag{48b}$$

For the simply supported edge:

$$c_1 = -\frac{F(1-F^2)}{2\pi \mathrm{i}}\frac{[I^{(2)}(0^-)]^2 - I(0^-)I^{(4)}(0^-)}{I^{(2)}(0^-)I^{(3)}(0^-) - I^{(1)}(0^-)I^{(4)}(0^-)}, \tag{49a}$$

$$c_2 = -\frac{F(1-F^2)}{2\pi}\frac{I^{(1)}(0^-)I^{(2)}(0^-) - I(0^-)I^{(3)}(0^-)}{I^{(2)}(0^-)I^{(3)}(0^-) - I^{(1)}(0^-)I^{(4)}(0^-)}. \tag{49b}$$

For the free edge:

$$c_1 = -\frac{F(1-F^2)}{2\pi \mathrm{i}}\frac{I^{(3)}(0^-)I^{(4)}(0^-) - I^{(2)}(0^-)I^{(5)}(0^-)}{[I^{(4)}(0^-)]^2 - I^{(3)}(0^-)I^{(5)}(0^-)}, \tag{50a}$$

$$c_2 = -\frac{F(1-F^2)}{2\pi}\frac{[I^{(3)}(0^-)]^2 - I^{(2)}(0^-)I^{(4)}(0^-)}{[I^{(4)}(0^-)]^2 - I^{(3)}(0^-)I^{(5)}(0^-)}. \tag{50b}$$

The value of $I^{(n)}(0^-)$ can be referenced to Eqs. (A2a) and (A10). Once c_0–c_3 are fully determined, the problem is fully solved. From Eq. (38), the horizontal velocity and hydrodynamic pressure can be ensured to be continuous in the water column beneath the plate edge.

As mentioned in Sec. III, additional Kutta conditions are needed to be imposed at the plate edge to ensure the uniqueness of the solution. This is in fact reflected by the cubic polynomial $Q(\alpha)$ in Eq. (44). For the former wave diffraction problem of a semi-infinite elastic plate [19,20], $Q(\alpha)$ is a linear function of α. Therefore, only two edge conditions can lead to a unique solution. This property further indicates the difference between these two types of problems.

As discussed in Sec. II, for linear stern waves behind a semi-infinite rigid plate [30], nontrivial solutions only exist for subcritical flows or $F < 1$. When $F > 1$, the vertical velocity at the plate edge will be infinity, which leads to the Kutta condition in Eq. (19b) not being satisfied, by contrast, since the elasticity of the plate is considered. It is interesting to see that a steady solution exists both at $F < 1$ and $F > 1$. From a physical perspective, traveling waves only exist in the downstream region ($x = +\infty$) at $F < 1$ for the rigid plate case. Here, traveling waves always exist in the fluid domain whether $F < 1$ or $F > 1$.

B. Far-field properties of the waves

To investigate the properties of waves at infinity, we may let $|x| \to +\infty$ in Eqs. (40), those terms of attenuation waves will be zero, and only the propagation waves will exist in the far field, which provides

$$\eta_1(x) = \begin{cases} -H(F-F_c)\frac{2\pi}{F}\frac{\sinh\kappa_{-1}[Q(\kappa_{-1})K_+(\kappa_{-1},F)e^{-\mathrm{i}\kappa_{-1}x}+Q(-\kappa_{-1})K_+(-\kappa_{-1},F)e^{\mathrm{i}\kappa_{-1}x}]}{\kappa_{-1}^2K_1'(\kappa_{-1},F)} & x \to -\infty \\ H(1-F)\frac{2\pi}{F}\frac{\sinh\mathscr{k}_0}{\mathscr{k}_0^2K_2'(\mathscr{k}_0,F)}\left[\frac{Q(\mathscr{k}_0)e^{-\mathrm{i}\mathscr{k}_0x}}{K_-(\mathscr{k}_0,F)} + \frac{Q(-\mathscr{k}_0)e^{\mathrm{i}\mathscr{k}_0x}}{K_-(-\mathscr{k}_0,F)}\right], & x \to +\infty. \end{cases} \tag{51}$$

Notice from Eqs. (47)–(50) that c_0 and c_2 are real and c_1 is imaginary, which gives $Q(-\alpha) = \bar{Q}(\alpha)$. Equations (30)–(32) also give $K_\pm(-\alpha, F) = \overline{K_\pm}(\alpha, F)$. Thus, Eqs. (51) can be further written as

$$\eta_1(x) = \begin{cases} -H(F-F_c)\frac{4\pi}{F}\frac{\sinh\kappa_{-1}}{\kappa_{-1}^2K_1'(\kappa_{-1},F)}\mathrm{Re}\{Q(\kappa_{-1})K_+(\kappa_{-1},F)e^{-\mathrm{i}\kappa_{-1}x}\}, & x \to -\infty \\ H(1-F)\frac{4\pi}{F}\frac{\sinh\mathscr{k}_0}{\mathscr{k}_0^2K_2'(\mathscr{k}_0,F)}\mathrm{Re}\left\{\frac{Q(\mathscr{k}_0)}{K_-(\mathscr{k}_0,F)}e^{-\mathrm{i}\mathscr{k}_0x}\right\}, & x \to +\infty. \end{cases} \tag{52}$$

Equations (52) further illustrate the distribution of waves at infinity. When $F < F_c$, there is only one wave component $\mathscr{k}_0$ at $x = +\infty$. When $F_c < F < 1$, one extra wave component κ_{-1} presents at $x = -\infty$. When $F > 1$, the wave component $\mathscr{k}_0$ disappears from $x = +\infty$, but the κ_{-1} remains

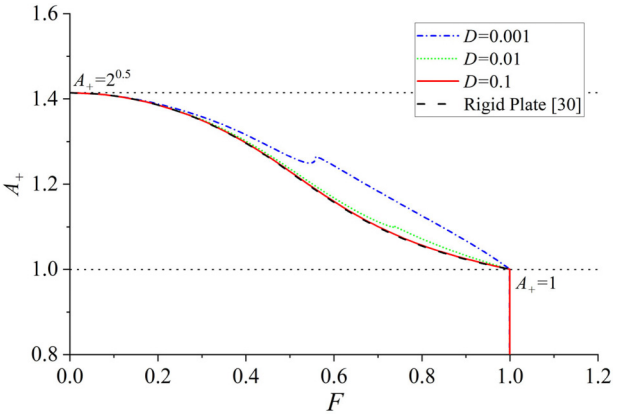

FIG. 6. The amplitude of the wave at $x = +\infty$ versus F (clamped edge condition).

at $x = -\infty$. We may further define the amplitude $A_\pm$ of the periodic waves at $x = \pm\infty$, which is similar to the wave reflection and transmission coefficients [19,20] in the periodic wave problem and is used to reflect the wave energy at the far field. From Eqs. (52), we may define

$$A_- = H(F - F_c)\frac{4\pi}{F}\frac{\sinh\kappa_{-1}}{\kappa_{-1}^2|K_1'(\kappa_{-1}, F)|}|Q(\kappa_{-1})K_+(\kappa_{-1}, F)|, \tag{53a}$$

$$A_+ = H(1 - F)\frac{4\pi}{F}\frac{\sinh\kappa_0}{\kappa_0^2|K_2'(\kappa_0, F)|}\left|\frac{Q(\kappa_0)}{K_-(\kappa_0, F)}\right|. \tag{53b}$$

It would be also interesting to see the asymptotic properties of $A_\pm$ at special values of F, or $F \to 0^+$, $F \to F_c + 0^\pm$, and $F \to 1$. When $F \to 0^+$, we may apply the derived asymptotic expression in Eqs. (B3a), (B6), and (B10) to Eq. (53b), and we obtain

$$A_+ \to \sqrt{2}, \quad F \to 0^+, \tag{54}$$

which is consistent with the case of a rigid plate in Ref. [24]. When $F \to F_c$, as proved in Eq. (B14) that $I^{(n)}(0^-)$ is continuous at $F = F_c$, together with Eqs. (48)–(50), we obtain that c_1 and c_2 should also be continuous at $F = F_c$. Furthermore, from Eqs. (44) and (53), it can be confirmed that A_- is bounded and A_+ is continuous at $F = F_c$. When $F \to 1$, we may substitute Eqs. (B15)–(B19) into Eqs. (53), which provides

$$A_- \to 0, \quad F \to 1^\pm, \tag{55a}$$

$$A_+ \to 1, \quad F \to 1^-. \tag{55b}$$

V. RESULTS AND DISCUSSION

In the following computations, all results will be presented in nondimensionalized forms as given in Sec. III. The results are obtained by truncating the infinite series in Eqs. (30) and (40) at $m = 1000$, which has been confirmed to be convergent.

A. Steady waves generated by an incoming current

Here, we may first consider the property of wave amplitude at infinity. From Eqs. (53), it can be known that $A_- = 0$ when $F < F_c$ and $A_+ = 0$ when $F > 1$. The result of A_+ versus F at different values of D is given in Fig. 6, where the edge condition at $x = 0$ and $z = 0$ is clamped. It is found that with the increase of the flexural rigidity, A_+ gradually tends to that of a rigid plate [30], which confirms that the present solution is consistent with the previous one when $D \to +\infty$.

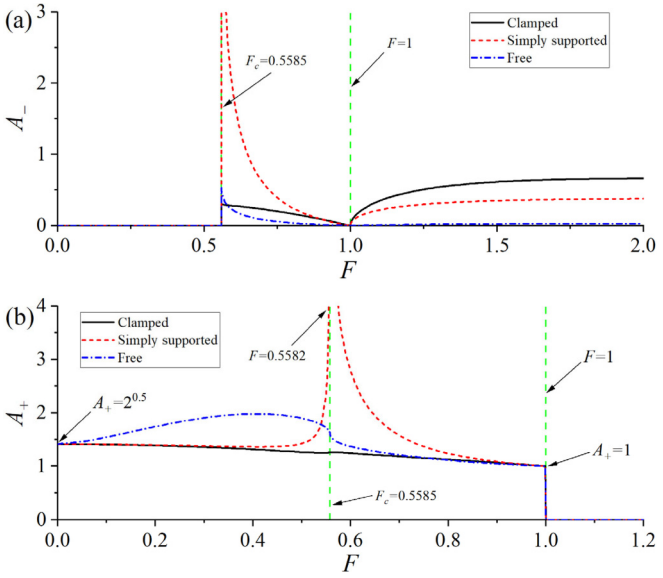

FIG. 7. The amplitude of the waves at $x = \pm\infty$ versus F ($D = 0.001$).

The results of $A_\pm$ versus F under different edge conditions are shown in Fig. 7, where $D = 0.001$. In Fig. 7(b), it is observed that $A_+ \to \sqrt{2}$ when $F \to 0^+$, which is consistent with the result in Eqs. (54). As F increases, when F is small, the magnitudes of A_+ under simply supported and clamped edges are quite similar, while A_+ under the free edge is significantly different. When F gradually approaches F_c, a sudden increase can be observed on the curve corresponding to the simply supported edge, and a very large peak is observed on A_+ at $F = 0.5582$, which occurs before $F_c = 0.5585$ but very close to it. The reason for such a peak is relevant and similar to the resonance of the motion and deformation of the elastic plate [43], which in fact can be seen as a local maximum response at a certain external excitation. In particular, at some values of F, the denominators of c_1 and c_2 in Eqs. (49a) and (49b) may be very small, and result in very large values of c_1, c_2, and A_+. For convenience, we may define such values of F as resonant Froude numbers, which are similar to the resonant frequencies corresponding to the vibration of an elastic plate. Here, $|c_1|$ and $|c_2|$ versus

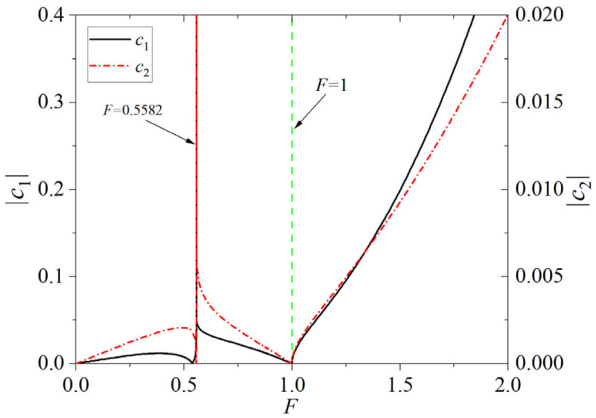

FIG. 8. Coefficients $|c_1|$ and $|c_2|$ versus F ($D = 0.001$, simply supported edge condition).

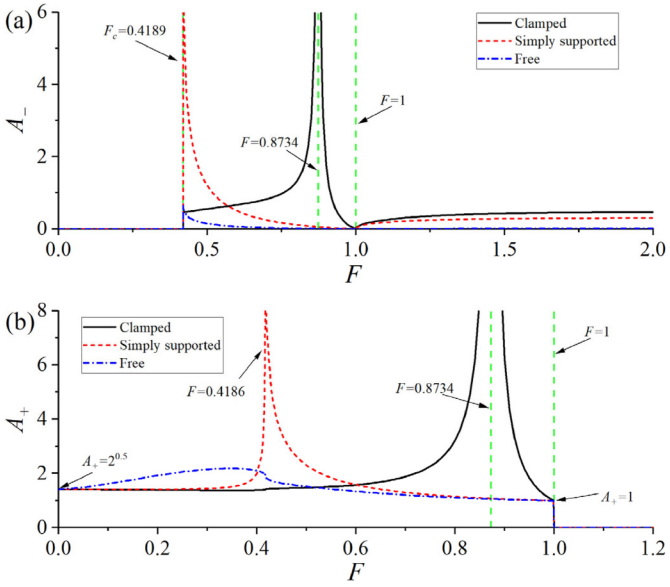

FIG. 9. The amplitude of the waves at $x = \pm\infty$ versus F ($D = 0.0001$).

F are plotted in Fig. 8 to clearly show how they behave at this resonant Froude number, and very large peaks are found at $F = 0.5582$ as expected.

When F continues to increase, there will be a sudden jump on A_- making A_- nonzero when F exceeds F_c, especially in the case of the simply supported edge, as shown in Fig. 7(a). As proved in Sec. IV B, A_- is bounded and A_+ is continuous at $F = F_c$, which is consistent with the results shown in Fig. 7. Besides, since $F_c = 0.5585$ is quite close to the above resonant Froude number $F = 0.5582$, as a result, $A_\pm$ at $F = F_c$ under simply supported edges is much larger than that under the other two edge conditions. As F continues to increase, $A_\pm$ gradually decreases. When $F \to 1$, it can be found that $A_- \to 0$ and $A_+ \to 1$ as predicted in Eqs. (55). After $F > 1$, A_+ is zero due to no propagation wave existing in the free surface region. By contrast, A_- slowly increases with F. Besides, at a fixed value of F, A_- increases in the following sequence: free, simply supported, and clamped.

In Fig. 7, the resonance behavior is only observed under the simply supported edge condition. Next, we may consider whether such a phenomenon can occur under the other two types of edge conditions. For the free-edge condition, the denominator of Eqs. (50) and (A11) give

$$[I^{(4)}(0^-)]^2 - I^{(3)}(0^-)I^{(5)}(0^-) = \frac{4\pi^2}{F^2D^2}, \tag{56}$$

which means that no peak value occurs. In such a case, the resonance cannot happen at the free-edge condition. To investigate the resonance phenomenon under the clamped edge condition, a softer elastic plate with $D = 0.0001$ is considered, where $A_\pm$ versus F is shown in Fig. 9. It can be found that very large peaks can be observed on A_+ and A_- at $F = 0.8734$ under the clamped edge condition. Besides, a similar peak is also found in A_+ at $F = 0.4186$ under the simply supported edge condition. Figures 7 and 9 show that the resonance phenomenon can occur under both simply supported and clamped edge conditions. The resonant Froude number for the simply supported edge is normally slightly smaller than F_c. By contrast, the resonant Froude number for the clamped edge is sensitive to the flexural rigidity D of the plate. In particular, the resonance is not observed here in Fig. 7 for $D = 0.001$, while the resonant Froude number is between $F = F_c$ and $F = 1$ in Fig. 9

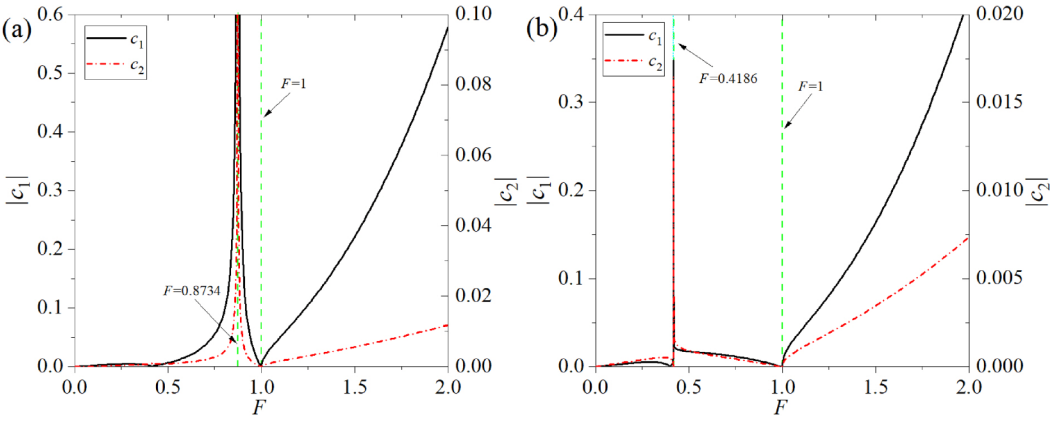

FIG. 10. Coefficients $|c_1|$ and $|c_2|$ versus F ($D = 0.0001$): (a) clamped edge and (b) simply supported edge.

for $D = 0.0001$. $|c_1|$ and $|c_2|$ versus F under clamped and simply supported edges are also given in Fig. 10 to verify that these peaks in Fig. 9 are due to resonance.

We may also consider the steady wave profiles, which can be calculated from

$$\eta(x) = \begin{cases} \eta_1(x) - 1, & x < 0 \\ \eta_1(x), & x > 0, \end{cases} \tag{57}$$

where $\eta_1(x)$ is given in Eqs. (40). $\eta(x)$ near $F_c = 0.4186$ under the simply supported edge condition is shown in Fig. 11. It can be observed that the amplitude of the wave varies very rapidly near the resonant Froude number; only a small change in F can lead to an obvious change in the wave profile, especially at $x > 0$. Similar phenomena can be also observed in the wave profile near $F_c = 0.8734$ under the clamped edge condition, as presented in Fig. 12. In addition to the wave amplitudes, rapid changes are also observed in the wave phase, as given in Figs. 11 and 12. It should be noted that the wave profiles obtained by the linearized velocity potential may not be accurate if the wave amplitude is too large. However, the prediction of the resonant Froude number itself may still be accurate and can be used to reflect the variation trend of the wave.

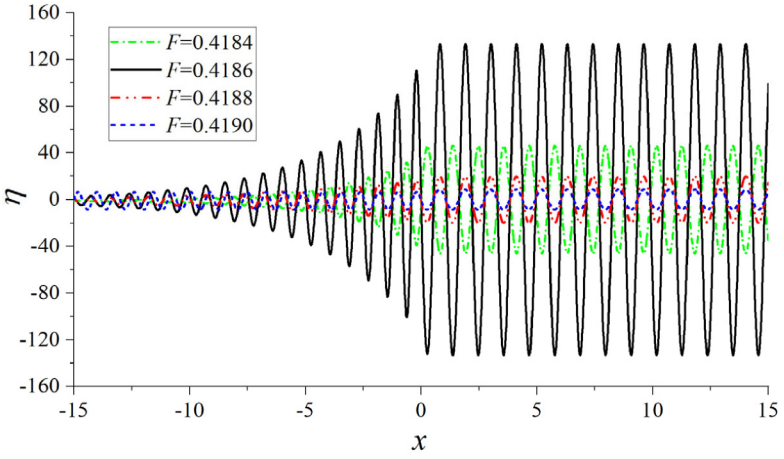

FIG. 11. The wave profile near the resonance Froude number under the simply supported edge ($D = 0.0001$).

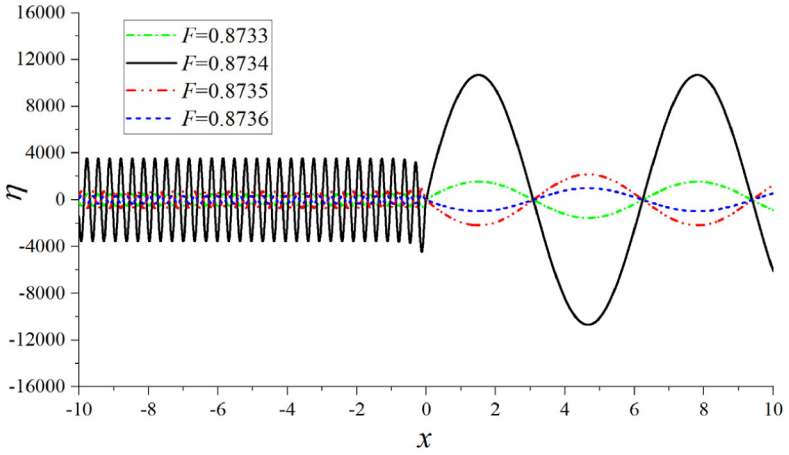

FIG. 12. The wave profile near the resonance Froude number under the clamped edge ($D = 0.0001$).

In order to clearly show how the edge conditions affect the steady wave profiles, we may consider $\eta(x)$ under $F = 0.2$, 0.6, and 1.2 here, as presented in Fig. 13. In Fig. 13(a) for $F = 0.2 < F_c$, the waves decay very rapidly at $x < 0$ in all three cases, while the main difference is in the wave amplitude at $x > 0$. In Fig. 13(b) for $F_c < F = 0.6 < 1$, the wave amplitude at $x < 0$ under the free-edge condition is much smaller than that of the other two edge conditions. Besides, obvious differences can be also observed in the wave phases. For the wave profile at $F = 1.2 > 1$ provided in Fig. 13(c), it can be found that the wave profiles under clamped and simply supported edge conditions only exhibit small differences, but that under the free-edge condition is quite distinct. In particular, the wave amplitude is notably small at $x < 0$, resulting in the wave profiles appearing almost as smooth curves.

B. Principal strain in the elastic thin plate

The principal strain in the elastic thin plate can be calculated from [36]

$$\varepsilon_{xx}(x) = -\frac{\xi}{2}\frac{d^2\eta_1(x)}{dx^2}, \tag{58}$$

where ξ denotes the nondimensionalized thickness of the plate (dimensionless by H). Substituting Eq. (40a) into Eq. (58), we obtain

$$\varepsilon_{xx}x = -\xi\frac{\pi}{F}\sum_{\zeta\in R_+}\frac{Q(\zeta)K_+(\zeta,F)\sinh\zeta}{K_1'(\zeta,F)}e^{-i\zeta x}, \quad x < 0. \tag{59}$$

$|\varepsilon_{xx}|/\xi$ near a resonant Froude number under the clamped edge is shown in Fig. 14. Similar to the wave profiles presented in Fig. 12, a very large value of strain can be observed, which may cause significant damage to the structure of the floating elastic plate [44,45]. Besides, the rapid change phenomenon can be also found in $|\varepsilon_{xx}|/\xi$. This point is of significant importance to engineering. For example, for a reservoir of water depth 10 m, Fig. 14 indicates that the current speed should be away from $U = 8.65$ m/s; otherwise a critical load will be on the FPV coverage, which guides the choice of water-release rate for reservoirs partially covered by FPV. We may next consider the principal strain under different edge conditions; an example is given in Fig. 15. For $F = 0.2 < F_c$ shown in Fig. 15(a), the strain is only concentrated near $x = 0^-$ because of no propagation wave at $x \to -\infty$. The maximum strain occurs at $x = 0$ for the clamped edge. By contrast, the other two cases occur at positions near $x = 0$ since the edge conditions require $\epsilon_{xx}(0) = 0$. For $F = 0.6 > F_c$

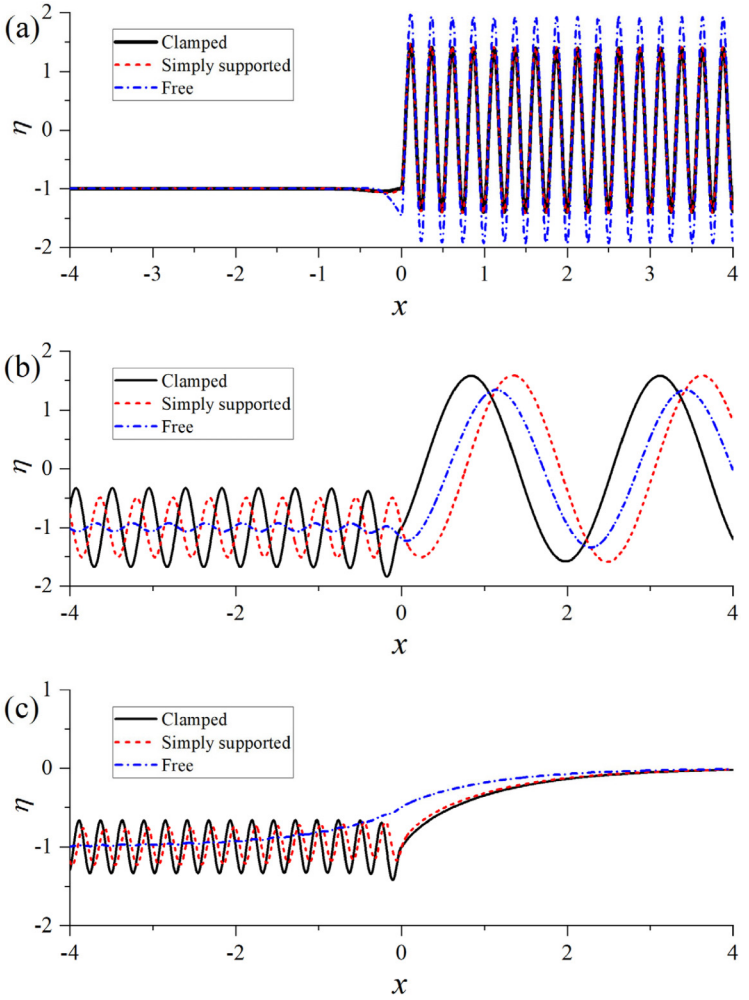

FIG. 13. Wave profiles at three different Froude numbers ($D = 0.0001$, $F_c = 0.4189$): (a) $F = 0.2$, (b) $F = 0.6$, and (c) $F = 1.2$.

in Fig. 15(b), it can be found that the strain under the free edge is much smaller than that under the other two edge conditions, which is similar to the wave elevation in Fig. 13(b).

VI. CONCLUSIONS

To study the underneath current effect on the edge of a floating solar farm, the problem of an incoming current interaction with a floating elastic thin plate of semi-infinite extent is analyzed. The fluid flow is described by the linearized velocity potential theory, while the elastic plate is modeled through a Kirchhoff-Love plate theory. The solution procedure is based on the Wiener-Hopf technique. When deriving the solution, the Kutta condition is applied to ensure the flow separates steadily from the lower edge of the plate, and the present analytical model is valid when the draft-based Froude number F_T is not low [39]. Letting the flexural rigidity of the plate $D \to +\infty$, the obtained results are verified by comparing with the previous study about the rigid plate [30].

A water depth Froude number is used to enable a nondimensionalized investigation of the problem. From the aspect of mathematics, when the elasticity of the plate is considered, nonsingular

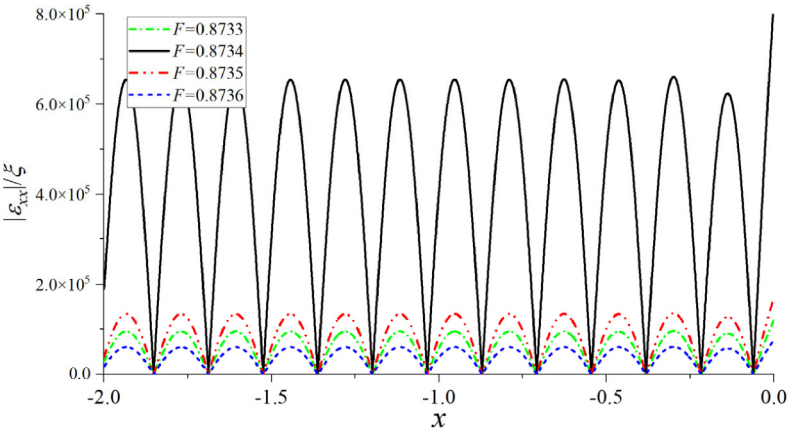

FIG. 14. The principal strain of the elastic plate near the resonance Froude number under the clamped edge ($D = 0.0001$).

solutions exist in the entire range of F, which is quite different from the rigid plate case, where the vertical velocity at the edge will be singular when $F > 1$.

The distribution of the propagation waves is analyzed in detail. When $F < F_c$, there is only a propagation wave at the free surface region ($x > 0$). When $F > F_c$, an extra propagation hydroelastic wave will show as the elastic plate deforms ($x < 0$). When $F > 1$, the propagation wave at $x > 0$ will disappear, while that at $x < 0$ remains. The behaviors of wave amplitudes $A_\pm$ at $x = \pm\infty$ are

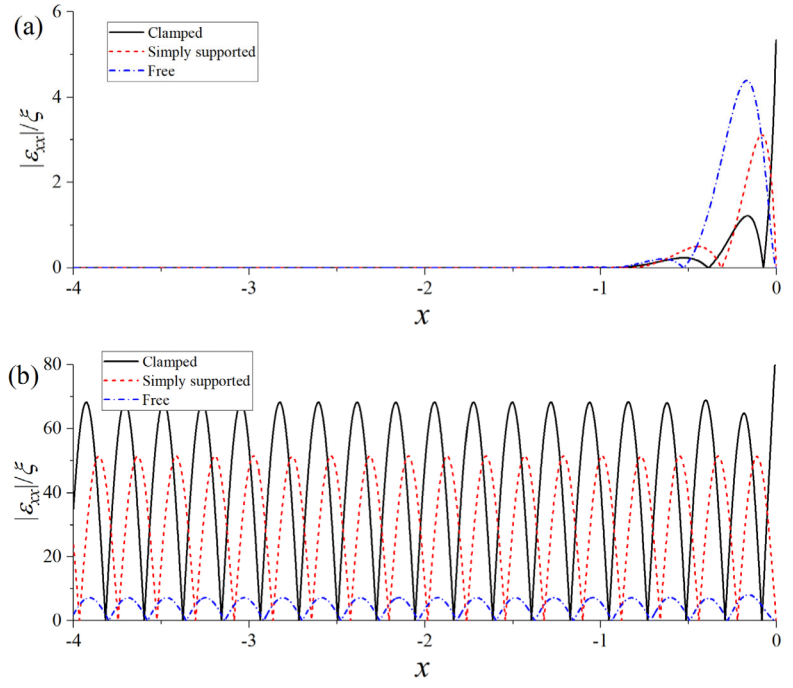

FIG. 15. The principal strain of the elastic plate at two different Froude numbers ($D = 0.0001$, $F_c = 0.4189$): (a) $F = 0.2$ and (b) $F = 0.6$.

also investigated. In particular, for A_+, it is proved mathematically that $A_+ \to \sqrt{2}$ when $F \to 0^+$ and $A_+ \to 1$ when $F \to 1^-$ for all three types of edge conditions. This phenomenon is consistent with the former rigid plate problem. It is also proved that A_+ is continuous at the critical Froude number F_c. Besides, A_- is normally bounded at $F = F_c$, and $A_- \to 0$ when $F \to 1$.

Moreover, we also observed another interesting phenomenon distinct from the rigid plate case. There may exist "resonant Froude numbers" under the clamped and simply supported edge conditions. In particular, near one of these Froude numbers, a phenomenon similar to wave resonance may occur, which makes the wave elevation and principal strain in the elastic plate significantly large. The physical mechanism can be elucidated through the examination of two coefficients related to edge conditions. When F approaches these resonant Froude numbers, these two coefficients exhibit significantly reduced denominators, consequently yielding significantly amplified results. However, it is worth noting that such resonance does not occur under free-edge conditions. The obtained results here provide valuable guidance for floating solar projects on water reservoirs to select their water-release rate and boundary conditions. For future work, we recommend using computational fluid dynamics and experiments to evaluate the accuracy of our results, as well as further investigation of the advanced fluid and structural features (e.g., turbulence, complex geometries) and nonlinear effects that are not covered by this analytic study.

ACKNOWLEDGMENTS

L.H. acknowledges grants received from Innovate UK (Grants No. 10048187, No. 10079774, and No. 10081314), the Royal Society (Grants No. IEC\NSFC\223253 and No. RG\R2\232462), and the UK Department for Transport (TRIG2023 Grant No. 30066).

APPENDIX A: COMPUTATION OF WAVE ELEVATION AND ITS DERIVATIVES AT THE PLATE EDGE

$I(x)$ in Eq. (46) can be converted into a series form by using the theorem of residue, which gives

$$I(x) = \begin{cases} -\frac{2\pi}{F}\sum_{\zeta\in R_+}\frac{K_+(\zeta,F)\sinh\zeta}{\zeta^2 K_1'(\zeta,F)}e^{-\mathrm{i}\zeta x}, & x<0 \\ \frac{2\pi}{F}\sum_{\zeta\in Q_-}\frac{\sinh\zeta}{\zeta^2 K_2'(\zeta,F)K_-(\zeta,F)}e^{-\mathrm{i}\zeta x}+\frac{2\pi}{F}\frac{1}{1-F^2}, & x>0 \end{cases}. \tag{A1a,b}$$

The derivative of $I(x)$ with respect to x at $x \to 0^{\pm}$ gives

$$I^{(n)}(0^-) = -\frac{2\pi(-\mathrm{i})^n}{F}\sum_{\zeta\in R_+}\frac{\zeta^{n-2}K_+(\zeta,F)\sinh\zeta}{K_1'(\zeta,F)}, \quad n\geqslant 0, \tag{A2a}$$

$$I^{(n)}(0^+) = \frac{2\pi(-\mathrm{i})^n}{F}\sum_{\zeta\in Q_-}\frac{\zeta^{n-2}\sinh\zeta}{K_2'(\zeta,F)K_-(\zeta,F)}+\delta_{n0}\frac{2\pi}{F}\frac{1}{1-F^2}, \quad n\geqslant 0, \tag{A2b}$$

where δ_{n0} denotes the Dirac delta function. From Eqs. (26), through some algebra, we can obtain

$$K_1'(\kappa_m,F) = \left[-F^2+\left(\frac{1}{F^2}-1\right)\frac{1}{\kappa_m^2}\right]\sinh\kappa_m, \tag{A3a}$$

$$K_2'(\kappa_m,F) = \left[\frac{D^2}{F^2}\kappa_m^6+\left(3D+\frac{2D}{F^2}\right)\kappa_m^2-F^2+\left(\frac{1}{F^2}-1\right)\frac{1}{\kappa_m^2}\right]\sinh\kappa_m, \tag{A3b}$$

which provides $\frac{\sinh\kappa_m}{K_1'(\kappa_m,F)} \sim O(m^6)$ and $\frac{\sinh(-\kappa_m)}{K_2'(-\kappa_m,F)} \sim O(m^0)$ as $m \to +\infty$. Besides, from Eqs. (30)–(32), we have $K_+(\kappa_m,F) \sim O(m^{0.5})$ and $K_-(\kappa_m,F) \sim O(m^{2.5})$ as $m \to +\infty$. Thus, the summation in $I^{(n)}(0^-)$ can be convergent for $n \leqslant 6$, but $I^{(n)}(0^+)$ only for $n \leqslant 3$. We may construct the following

contour integral for $n \leqslant 3$:

$$J_1 = \frac{(-\mathrm{i})^{n+1}}{F} \oint_{C_R} \frac{\zeta^{n-2} K_+(\zeta, F) \sinh \zeta}{K_1(\zeta, F)} d\zeta, \quad n \leqslant 3. \tag{A4}$$

where C_R is a circle of radius $R \to +\infty$. The integrand in Eq. (A4) is of $|\zeta|^{n-4.5}$ as $|\zeta| \to +\infty$, which means $J_1 = 0$. Applying the residue theorem, we have

$$\frac{2\pi(-\mathrm{i})^n}{F} \sum_{\zeta \in R_+} \frac{\zeta^{n-2} K_+(\zeta, F) \sinh \zeta}{K_1'(\zeta, F)} + \frac{2\pi(-\mathrm{i})^n}{F} \sum_{\zeta \in Q_-} \frac{\zeta^{n-2} \sinh \zeta}{K_2'(\zeta, F) K_-(\zeta, F)} + \delta_{n0} \frac{2\pi}{F} \frac{1}{1 - F^2} = 0, \quad n \leqslant 3. \tag{A5}$$

Hence, Eq. (A5) provides $I^{(n)}(0^-) = I^{(n)}(0^+)$ for $n \leqslant 3$. In Eq. (A2a), the summation may converge slowly, especially when n is large. An efficient way to work out the summation is to use the residue calculus technique [46]. Notice that

$$\sinh \zeta = -\frac{K_2(\zeta, F)}{D\zeta^3} \quad \text{if } \zeta \in R_+. \tag{A6}$$

$I^{(n)}(0^-)$ can be also expressed as

$$I^{(n)}(0^-) = \frac{2\pi(-\mathrm{i})^n}{FD} \sum_{\zeta \in R_+} \frac{\zeta^{n-5} K_+(\zeta, F) K_2(\zeta, F)}{K_1^{'}(\zeta, F)}. \tag{A7}$$

Constructing the following integral and using $K_2(\zeta, F)/K_1(\zeta, F) = K_+(\zeta, F) K_-(\zeta, F)$ provides

$$J_2 = \frac{1}{2\pi \mathrm{i}} \oint_{C_R} \frac{\zeta^{n-5} K_+(\zeta, F) K_2(\zeta, F)}{K_1(\zeta, F)} d\zeta = \frac{1}{2\pi \mathrm{i}} \oint_{C_R} \frac{\zeta^{n-5}}{K_-(\zeta, F)} d\zeta, \quad n \leqslant 6. \tag{A8}$$

The integrand in Eq. (A8) is of $|\zeta|^{n-7.5}$ as $|\zeta| \to +\infty$, which means $J_2 = 0$. Applying the theorem of residue to Eq. (A8) again, we obtain

$$\sum_{\zeta \in R_+} \frac{\zeta^{n-5} K_+(\zeta, F) K_2(\zeta, F)}{K_1^{'}(\zeta, F)} = -\mathrm{Res}\left\{ \frac{\zeta^{n-5}}{K_-(\zeta, F)}; \zeta = 0 \right\}. \tag{A9}$$

In such a case, the summation is converted into the residue of a function at $\zeta = 0$. Applying Eq. (A9) to Eq. (A7), we have

$$I^{(n)}(0^-) = -\frac{2\pi(-\mathrm{i})^n}{FD} \mathrm{Res}\left\{ \frac{\zeta^{n-5}}{K_-(\zeta, F)}; \zeta = 0 \right\}. \tag{A10}$$

When $n = 0$, 1, 2, the residue in Eq. (A10) is hard to work out analytically. Alternatively, we may use Eq. (A2a). By contrast, it is relatively straightforward to determine $I^{(3)}(0^-)$, $I^{(4)}(0^-)$, and $I^{(5)}(0^-)$ through Eq. (A10) as

$$I^{(3)}(0^-) = \frac{2\pi \mathrm{i}}{FD} \frac{K_-^{'}(0, F)}{K_-^2(0, F)} = \frac{2\pi \mathrm{i}}{FD} K_-^{'}(0, F) \tag{A11a}$$

$$I^{(4)}(0^-) = -\frac{2\pi}{FD} \frac{1}{K_-(0, F)} = -\frac{2\pi}{FD} \tag{A11b}$$

$$I^{(5)}(0^-) = 0. \tag{A11c}$$

APPENDIX B: BEHAVIORS OF SOME FUNCTIONS NEAR SPECIAL VALUES OF F

We may first consider the case when $F \to 0^+$. Equations (26) provide

$$K_1(\alpha, F) = 0 \Rightarrow (D\alpha^4 + 1)\frac{\tanh\alpha}{\alpha} = F^2 \to 0^+, \tag{B1a}$$

$$K_2(\alpha, F) = 0 \Rightarrow \frac{\tanh\alpha}{\alpha} = F^2 \to 0^+. \tag{B1b}$$

The roots of Eqs. (B1) when $F \to 0^+$ can be solved as follows: $\kappa_{-1} = -\bar{\kappa}_0 \to D^{-\frac{1}{4}} e^{\mathrm{i}\frac{\pi}{4}}$, $\mathscr{k}_0 \to \frac{1}{F^2} \to +\infty$, and $\kappa_m \approx \mathscr{k}_m \to m\pi\mathrm{i}$ $(m \geqslant 1)$. In such a case, $K_i^{'}(\kappa_m, F)$ $(i = 1, 2)$ can be expressed as

$$K_1^{'}(\kappa_m, F) \to 4D\kappa_m^2 \sinh\kappa_m, \quad m = -1,\ 0, \quad F \to 0^+ \tag{B2a}$$

$$K_1^{'}(\kappa_m, F) \to \left(D\kappa_m^4 + 1\right)\frac{\cosh\kappa_m}{\kappa_m}, \quad m \geqslant 1, \quad F \to 0^+. \tag{B2b}$$

$$K_2^{'}(\mathscr{k}_0, F) \to -\frac{\sinh\mathscr{k}_0}{\mathscr{k}_0^2}, \quad F \to 0^+ \tag{B3a}$$

$$K_2^{'}(\kappa_m, F) \to \frac{\cosh\mathscr{k}_m}{\mathscr{k}_m} \quad m \geqslant 1, \quad F \to 0^+. \tag{B3b}$$

Using the asymptotic behaviors of κ_m $(m \geqslant -1)$ and $\mathscr{k}_m$ $(m \geqslant 0)$, $K_\pm(\alpha, F)$ in Eq. (30) can be written as

$$K_-(\alpha, F) \to \frac{(\kappa_{-1} - \alpha)(\kappa_0 - \alpha)}{\kappa_{-1}\kappa_0}, \quad F \to 0^+ \tag{B4a}$$

$$K_+(\alpha, F) \to \frac{\mathscr{k}_0^2(\kappa_{-1} - \alpha)(\kappa_0 - \alpha)}{\kappa_{-1}\kappa_0\left(\mathscr{k}_0^2 - \alpha^2\right)}, \quad F \to 0^+. \tag{B4b}$$

Notice from Eqs. (30)–(32) we have

$$K_+(\alpha, F) = \frac{\mathscr{k}_0^2}{\mathscr{k}_0^2 - \alpha^2} K_-(-\alpha, F), \quad F < F_c. \tag{B5}$$

Substitute Eq. (B5) into Eq. (28), and notice $K_\pm(-\alpha, F) = \bar{K}_\pm(\alpha, F)$, which provides

$$|K_-(\mathscr{k}_0, F)| = \lim_{\alpha\to\mathscr{k}_0} \sqrt{K_-(-\alpha, F)K_-(\alpha, F)} = \lim_{\alpha\to\mathscr{k}_0} \sqrt{\frac{\mathscr{k}_0^2 - \alpha^2}{\mathscr{k}_0^2}\frac{K_1(\alpha, F)}{K_2(\alpha, F)}} = \sqrt{2D}\mathscr{k}_0^2. \tag{B6}$$

We may consider the following formulas and invoke Eqs. (B2):

$$\begin{aligned} &\frac{\kappa_m^{n-2}K_+(\kappa_m, F)\sinh\kappa_m}{K_1^{'}(\kappa_m, F)} \to \frac{\kappa_m^{n-4}K_+(\kappa_m, F)}{4D}, && m = -1,\ 0 \\ &\frac{\kappa_m^{n-2}K_+(\kappa_m, F)\sinh\kappa_m}{K_1^{'}(\kappa_m, F)} \to \frac{\kappa_m^{n-1}K_+(\kappa_m, F)\tanh\kappa_m}{\left(D\kappa_m^4 + 1\right) \to 0}, && m \geqslant 1, \end{aligned} \quad n \leqslant 5,\ F \to 0^+. \tag{B7}$$

Substituting Eqs. (B4) and (B7) into Eq. (A2a), as well as using the asymptotic behavior of κ_m $(m \geqslant -1)$, only the leading-order terms in $I^{(n)}(0^-)$ should be kept, which provides

$$\begin{aligned} I^{(n)}(0^-) &\to -\frac{\pi(-\mathrm{i})^n}{2DF}\left[\kappa_{-1}^{n-4}K_+(\kappa_{-1}, F) + \kappa_0^{n-4}K_+(\kappa_0, F)\right] \\ &\to \frac{\pi(-\mathrm{i})^n D^{-\frac{n}{4}}}{2F}\left[e^{\mathrm{i}\frac{(n-1)\pi}{4}} + e^{\mathrm{i}\frac{(3n+1)\pi}{4}}\right], \quad n \leqslant 5,\ F \to 0^+. \end{aligned} \tag{B8}$$

Applying Eq. (B8) to Eqs. (48)–(50), we have

$$c_1 \to -\frac{\sqrt{2}F}{2\pi \mathrm{i}} D^{\frac{1}{4}} \quad \text{as } F \to 0^+ \tag{B9a}$$

$$c_2 \to -\frac{F}{2\pi} D^{\frac{1}{2}} \quad \text{as } F \to 0^+, \tag{B9b}$$

and together with Eq. (44), we further obtain

$$Q(\mathscr{k}_0) \to -\frac{F}{2\pi} \mathscr{k}_0^2 D^{\frac{1}{2}}. \tag{B10}$$

Next, we may consider the situation when $F \to F_c$, which provides $\kappa_{-1} \to \kappa_c$ and $\kappa_0 \to \kappa_c$, where κ_c denotes the unique positive real root of $K_1(\alpha, F_c) = 0$ as mentioned in Sec. IV A. Applying the Taylor series to $K_1(\alpha, F) = 0$ at $\alpha = \kappa_c$ and $F = F_c$, κ_{-1} and κ_0 can be expressed in the following asymptotic way:

$$\kappa_{-1} = \kappa_c + \mathrm{i}\sigma, \kappa_0 = -\kappa_c + \mathrm{i}\sigma, \quad F \to F_c + 0^- \tag{B11a}$$

$$\kappa_{-1} = \kappa_c + \sigma, \kappa_0 = \kappa_c - \sigma, \quad F \to F_c + 0^+, \tag{B11b}$$

where

$$\sigma = 2\sqrt{\frac{F_c \cosh \alpha_c}{K_1''(\kappa_c, F_c)} |F - F_c|} \to 0^+, \tag{B12}$$

and From Eqs. (26a) and (B11), we have $K_1'(\kappa_{-1}, F)$ as

$$K_1'(\kappa_{-1}, F) = K_1''(\kappa_c, F_c)\mathrm{i}\sigma \quad F \to F_c + 0^- \tag{B13a}$$

$$K_1'(\kappa_{-1}, F) = K_1''(\kappa_c, F_c)\sigma \quad F \to F_c + 0^+ \tag{B13b}$$

Substituting Eqs. (B11) and (B13) into Eq. (A2a), after some algebra, we obtain

$$I^{(n)}(0^-) = -\frac{2\pi(-\mathrm{i})^n}{F_c} \left\{ \frac{4\mathscr{k}_0^2 \kappa_c^{n-3} \sinh \kappa_c}{(\mathscr{k}_0^2 - \kappa_c^2) K_1''(\kappa_c, F_c)} \left[\prod_{m=1}^{+\infty} \left[\frac{\mathscr{k}_m(\kappa_m - \kappa_c)}{\kappa_m(\mathscr{k}_m - \kappa_c)} \right] \right. \right.$$
$$\left. \left. - \prod_{m=1}^{+\infty} \left[\frac{\mathscr{k}_m(\kappa_m + \kappa_c)}{\kappa_m(\mathscr{k}_m + \kappa_c)} \right] \right] + \sum_{m=1}^{+\infty} \frac{\kappa_m^{n-2} K_+(\kappa_m, F) \sinh \kappa_m}{K_1'(\kappa_m, F)} \right\}, \quad F \to F_c + 0^{\pm}, \tag{B14}$$

which proves that $I^{(n)}(0^-)$ is continuous at $F = F_c$.

We may finally consider the case when $F \to 1$, which provides $\mathscr{k}_0 \to 0$ and $\kappa_0 \to 0$. Applying the Taylor series to $K_i(\alpha, F) = 0$ $(i = 1, 2)$ at $\alpha = 0$ and $F = 1$, we obtain

$$\mathscr{k}_0^2 \to 3(1 - F^2), \quad F \to 1. \tag{B15a}$$

$$\kappa_0^2 \to 3(1 - F^2), \quad F \to 1 \tag{B15b}$$

$$K_2'(\mathscr{k}_0, F) \to -\tfrac{2}{3}\mathscr{k}_0, \quad F \to 1. \tag{B16}$$

Substituting Eqs. (B15) into Eqs. (30)–(32), we have

$$K_-(\mathscr{k}_0, F) \to 1 \tag{B17a}$$

$$K_+(\kappa_{-1}, F) \to \prod_{m=1}^{+\infty} \left[\frac{\mathscr{k}_m(\kappa_m + \kappa_{-1})}{\kappa_m(\mathscr{k}_m + \kappa_{-1})} \right]. \tag{B17b}$$

Equation (A2a) confirms that $I^{(n)}(0^-)$ is bounded when $F \to 1$; furthermore, from Eqs. (48)–(50) we obtain

$$c_i = O((1-F^2)), \quad i = 0 \sim 2, \quad F \to 1. \tag{B18}$$

In such a case, applying Eqs. (B15a) and (B18) to Eq. (44), we may write

$$\begin{aligned} Q(\kappa_0) &= \frac{F(1-F^2)}{2\pi} + O((1-F^2)^{3/2}) \\ Q(\kappa_{-1}) &= O((1-F^2)), \end{aligned} \quad , \quad F \to 1. \tag{B19}$$

[1] J. Van Zalk and P. Behrens, The spatial extent of renewable and non-renewable power generation: A review and meta-analysis of power densities and their application in the US, Energy Policy **123**, 83 (2018).

[2] N. Lee, U. Grunwald, E. Rosenlieb, H. Mirletz, A. Aznar, R. Spencer, and S. Cox, Hybrid floating solar photovoltaics-hydropower systems: Benefits and global assessment of technical potential, Renewable Energy **162**, 1415 (2020).

[3] J. Dai, C. Zhang, H. V. Lim, K. K. Ang, X. Qian, J. L. H. Wong, S. T. Tan, and C. L. Wang, Design and construction of floating modular photovoltaic system for water reservoirs, Energy **191**, 116549 (2020).

[4] R. M. Almeida, Floating solar power could help fight climate change—let's get it right, Nature (London) **606**, 246 (2022).

[5] S. Oliveira-Pinto and J. Stokkermans, in *Proceedings of the Institution of Civil Engineers-Maritime Engineering* (Thomas Telford, 2020), p. 120.

[6] J. V. Wehausen and E. V. Laitone, in *Fluid Dynamics/Strömungsmechanik* (Springer, Berlin, 1960), p. 446.

[7] L. Huang, K. Ren, M. Li, Ž. Tuković, P. Cardiff, and G. Thomas, Fluid-structure interaction of a large ice sheet in waves, Ocean Eng. **182**, 102 (2019).

[8] Y. F. Yang, G. X. Wu, and K. Ren, Three-dimensional interaction between uniform current and a submerged horizontal cylinder in an ice-covered channel, J. Fluid Mech. **928**, A4 (2021).

[9] Y. F. Yang, G. X. Wu, and K. Ren, Hydroelastic wave diffraction by a vertical circular cylinder standing in a channel with an ice cover, J. Fluid Mech. **941**, A13 (2022).

[10] D. K. Sree, A. W.-K. Law, D. S. C. Pang, S. T. Tan, C. L. Wang, J. H. Kew, W. K. Seow, and V. H. Lim, Fluid-structural analysis of modular floating solar farms under wave motion, Sol. Energy **233**, 161 (2022).

[11] S. Delacroix, S. Bourdier, T. Soulard, H. Elzaabalawy, and P. Vasilenko, Experimental modelling of a floating solar power plant array under wave forcing, Energies **16**, 5198 (2023).

[12] Y. J. Wei, Motion characteristics of a modularized floating solar farm in waves, Phys. Fluids **36**, 033320 (2024).

[13] S. M. Zheng, S. Michele, H. Liang, M. H. Meylan, and D. Greaves, Wave power extraction from a floating elastic disk-shaped wave energy converter, J. Fluid Mech. **948**, A38 (2022).

[14] C. Bi and A. W.-K. Law, Co-locating offshore wind and floating solar farms–effect of high wind and wave conditions on solar power performance, Energy **266**, 126437 (2023).

[15] C. W. Zhang, P. F. Wang, L. F. Huang, M. K. Zhang, H. T. Wu, and D. Z. Ning, Resonance mechanism of hydroelastic response of multi-patch floating photovoltaic structure in water waves over stepped seabed, Phys. Fluids **35**, 107137 (2023).

[16] Y. F. Yang, K. Ren, B. Z. Zhou, S. Y. Sun, and L. F. Huang, Wave interaction with multiple adjacent floating solar panels with arbitrary constraints, Phys. Fluids **36**, 037121 (2024).

[17] C. Fox and V. A. Squire, Reflection and transmission characteristics at the edge of shore fast sea ice, J. Geophys. Res.: Oceans **95**, 11629 (1990).

[18] T. Sahoo, T. L. Yip, and A. T. Chwang, Scattering of surface waves by a semi-infinite floating elastic plate, Phys. Fluids **13**, 3215 (2001).

[19] N. J. Balmforth and R. V. Craster, Ocean waves and ice sheets, J. Fluid Mech. **395**, 89 (1999).

[20] L. A. Tkacheva, Scattering of surface waves by the edge of a floating elastic plate, J. Appl. Mech. Tech. Phys. **42**, 638 (2001).
[21] B. Noble, *Methods Based on the Wiener-Hopf Technique for the Solution of Partial Differential Equations* (Pergamon Press, London, 1958).
[22] A. I. Andrianov and A. J. Hermans, Hydroelastic analysis of a floating plate of finite draft, Appl. Ocean Res. **28**, 313 (2006).
[23] H. J. Haussling, Two-dimensional linear and nonlinear stern waves, J. Fluid Mech. **97**, 759 (1980).
[24] G. H. Schmidt, Linearized stern flow of a two-dimensional shallow-draft ship, J. Ship Res. **25**, 236 (1981).
[25] J. W. Davys, R. J. Hosking, and A. D. Sneyd, Waves due to a steadily moving source on a floating ice plate, J. Fluid Mech. **158**, 269 (1985).
[26] F. Milinazzo, M. Shinbrot, and N. W. Evans, A mathematical analysis of the steady response of floating ice to the uniform motion of a rectangular load, J. Fluid Mech. **287**, 173 (1995).
[27] P. Guyenne and E. I. Parau, Computations of fully nonlinear hydroelastic solitary waves on deep water, J. Fluid Mech. **713**, 307 (2012).
[28] Z. F. Li, G. X. Wu, and Y. Y. Shi, Interaction of uniform current with a circular cylinder submerged below an ice sheet, Appl. Ocean Res. **86**, 310 (2019).
[29] C. J. Lustri, Exponential asymptotics for elastic and elastic-gravity waves on flow past submerged obstacles, J. Fluid Mech. **950**, A6 (2022).
[30] S. W. McCue and D. M. Stump, Linear stern waves in finite depth channels, Q. J. Mech. Appl. Math. **53**, 629 (2000).
[31] M. Maleewong and R. H. J. Grimshaw, Nonlinear free surface flows past a semi-infinite flat plate in water of finite depth, Phys. Fluids **20**, 062102 (2008).
[32] B. J. Binder, Steady free-surface flow at the stern of a ship, Phys. Fluids **22**, 012104 (2010).
[33] O. Ogilat, S. W. McCue, I. W. Turner, J. A. Belward, and B. J. Binder, Minimising wave drag for free surface flow past a two-dimensional stern, Phys. Fluids **23**, 072101 (2011).
[34] M. W. Pierce, Y. M. Liu, and D. K. P. Yue, Sum-frequency triad interactions among surface waves propagating through an ice sheet, J. Fluid Mech. **980**, A45 (2024).
[35] A. Sahu, N. Yadav, and K. Sudhakar, Floating photovoltaic power plant: A review, Renewable Sustainable Energy Rev. **66**, 815 (2016).
[36] S. P. Timoshenko and S. Woinowsky-Krieger, *Theory of Plates and Shells* (McGraw-Hill, New York, 1959).
[37] M. Reinhard, A. Korobkin, and M. Cooker, Water entry of a flat elastic plate at high horizontal speed, J. Fluid Mech. **724**, 123 (2013).
[38] J. N. Newman, *Marine Hydrodynamics* (MIT Press, Cambridge, MA, 2018).
[39] K. J. Maki, *Transom Stern Hydrodynamics* (University of Michigan, 2006).
[40] P. Novak, A. Moffat, C. Nalluri, and R. Narayanan, *Hydraulic Structures* (CRC Press, Boca Raton, FL, 2017).
[41] Y. F. Yang, G. X. Wu, and K. Ren, Interaction between a uniform current and a submerged cylinder in a marginal ice zone, J. Fluid Mech. **984**, A50 (2024).
[42] T. H. Havelock, The forces on a circular cylinder submerged in a uniform stream, Proc. R. Soc. London Ser. A Math. Phys. Sci. **157**, 526 (1936).
[43] A. G. Piersol and T. L. Paez, *Harris' Shock and Vibration Handbook*, 6th ed. (McGraw-Hill Education, New York, 2010).
[44] J. Ong, K. Tay, and H. Hammer, Technical considerations to ensuring bankable floating PV projects, PV Tech Power, Vol. 24, https://solar-media.s3.amazonaws.com/assets/Pubs/PVTP24/Technical%20considerations%20to%20ensuring%20bankable%20floating%20PV%20projects.pdf.
[45] H. P. Markieh, A. K. Hendukhale, M. Khorasanchi, and E. Oguz, A review on conceptual design of support structures for floating solar power plants, in *7th Offshore Energy & Storage Symposium (OSES 2023)* (Institution of Engineering and Technology, 2023), pp. 80–86.
[46] T. D. Williams and V. A. Squire, Scattering of flexural–gravity waves at the boundaries between three floating sheets with applications, J. Fluid Mech. **569**, 113 (2006).